Talanta 114 (2013) 183–190

Contents lists available at ScienceDirect

Talanta

journal homepage: www.elsevier.com/locate/talanta

Visible-light-driven photocatalytic and chemical sensing properties of SnS_2 nanoflakes

Ahmad Umar [a,b,*], M.S. Akhtar [c], G.N. Dar [b,e], M. Abaker [b,e], A. Al-Hajry [b,d], S. Baskoutas [e]

[a] Department of Chemistry, College of Science and Arts, Najran University, P.O. Box 1988, Najran 11001, Kingdom of Saudi Arabia
[b] Promising Centre for Sensors and Electronic Devices (PCSED), Najran University, P.O. Box 1988, Najran 11001, Kingdom of Saudi Arabia
[c] New and Renewable Energy Materials Development Center (NewREC), Chonbuk National University, Jeonbuk, South Korea
[d] Department of Physics, Faculty of Sciences and Arts, Najran University, P.O. Box 1988, Najran-11001, Kingdom of Saudi Arabia
[e] Department of Materials Science, University of Patras, Patras, Greece

ARTICLE INFO

Article history:
Received 4 February 2013
Received in revised form
19 March 2013
Accepted 20 March 2013
Available online 28 March 2013

Keywords:
SnS_2
Nanoflakes
Photocatalytic degradation
Rhodamine B
Nitroaniline
Chemical sensors

ABSTRACT

This work demonstrated the successful and facile large-scale synthesis and characterizations of SnS_2 nanoflakes. The detailed morphological studies revealed that the synthesized products were nanoflakes and were grown in large quantity. The XRD pattern and detailed compositional studies confirmed that the synthesized SnS_2 nanoflakes were well-crystalline and possessing hexagonal SnS_2 phase. The synthesized SnS_2 nanoflakes were used as efficient photocatalysts for photocatalytic degradation and effective electron mediators for the fabrication of chemical sensor. The photocatalytic properties of SnS_2 nanoflakes towards the photocatalytic degradation of Rhodamine B dye under visible light irradiation showed reasonably good degradation of ~61%. Moreover, the as-synthesized SnS_2 nanoflakes were used as efficient electron mediators for the fabrication of nitroaniline chemical sensor by simple *I-V* technique. Very high-sensitivity of $\sim 505.82 \pm 0.02\ mAcm^{-2}.(mole/L)^{-1}$ and experimental detection limit of $\sim 15 \times 10^{-6}$ (mole/L) in a short response time of ~10.0 s with LDR in the range of 15.6×10^{-6}–0.5×10^{-3} mole L^{-1} were observed for the fabricated nitroaniline chemical sensor. The observed results indicated that the SnS_2 nanoflakes can efficiently be used as visible-light-driven photocatalysts and the fabrication of ultra-high sensitive chemical sensors.

1. Introduction

The aquatic environmental imbalance mainly occurs by the contamination of water with the harmful non-biodegradable materials [1–3]. Various textile and chemical industries release many harmful organic macromolecules and dyes [4,5]. Particularly the disposable of colored organic waste water from the textile dyeing industries causes a serious problem to aquatic ecosystem and hence contaminate the environment which cause a serious threat to the living organisms [6]. Among various water soluble dyes, Rhodamine B (RhB) with non-volatile nature and bright reddish violet in color are extensively used in various prospect applications such as fluorescence microscopy, flow cytometry, fluorescence correlation spectroscopy and ELISA [7] and also applied for dying cottons, bamboo, weed, stamp pad inks etc. The waste of RhB dye hazardously affects natural environments especially aquatic life and lead the mutagenic effects to humans and other living organisms [8,9]. Conventionally, a biological treatment or degradation process utilizes to decolorize the dyes, but it is ineffective for the complete removal and degradation of dye. Last few years, the catalytic process derived by solar energy or other radiation energy has been studied for the successful degradation of harmful organic dyes into environmental friendly materials [10]. In this regard, because of the unique band gap and various other physical and chemical properties, the nanoscale inorganic semiconductors such as metal oxides, metal sulfides etc. were used as active catalysts for the degradation/oxidation of organic dyes and reported in the literature [11]. The photocatalytic degradation occurs due to the effective separation of excited electron in conduction band (CB) and hole in valance band (VB) under the light illumination, which could capture by some surface species in the surroundings such as hydroxyl or O_2 groups [12]. These catalysts are usually active under the UV-light. Among various semiconducting materials, the metal sulfides have received a great deal of interest as promising photocatalysts under

* Corresponding author at: Najran University, Centre for Advanced Materials and Nanoengineering (CAMNE), Centre for Advanced Materials and Najran 11001, Saudi Arabia. Tel.: +966 534 574597.
E-mail address: ahmadumar786@gmail.com (A. Umar).

0039-9140/$ - see front matter © 2013 Elsevier B.V. All rights reserved.
http://dx.doi.org/10.1016/j.talanta.2013.03.050

the visible light illumination [13]. Domen et al. demonstrated a high photo-activity for hydrogen evolution over the surface of synthesized nanostructured CdS under visible light [14].

Recently, the IV–VI group semiconductors such as tin sulfides (SnS, SnS_2) have received much attention owing to their strong anisotropy of optical properties and potential applications in solar cells as well as electrical switchings [15–20]. Among large number of binary tin sulfides (SnS, SnS_2, Sn_2S_3, Sn_3S_4, Sn_4S SnS and SnS_2), the SnS_2 possesses special place due to its own properties and wide applications in solar cells, lithium-ion batteries, optoelectronics, photoluminescence and so on [21]. The SnS_2 is an *n*-type semiconductor and is receiving much attention owing to its layered hexagonal CdI_2-type crystal structure with two layers of close-packed sulfur anions and tin cations sandwiched between them in an octahedral coordination manner. Due to its absorption tunable band gap of 2.2 eV, the crystalline SnS_2 could be a promising photocatalytic material for the photocatalytic degradation of organic dyes in the presence of visible-light [22]. Moreover, SnS_2 nanomaterials possess good oxidative and thermal stability in acid and neutral environment [23,24].

In this work, we demonstrate the facile and large-scale synthesis of well-crystalline SnS_2 nanoflakes by simple hydrothermal process. The synthesized nanoflakes were characterized in detail in terms of their morphological, structural and compositional properties. The as-synthesized nanoflakes were used as efficient photocatalysts for photocatalytic degradation of Rhodamine B dye under visible light. Moreover, the prepared nanoflakes were used as efficient electron mediators for the fabrication of nitroaniline chemical sensor by simple *I–V* technique.

2. Experimental details

2.1. Synthesis of SnS_2 nanoflakes

All the chemicals utilized for the synthesis of SnS_2 nanoflakes were purchased from Sigma-Aldrich and used without further purification. Distilled water (DW) was used for all the synthesis process. Well-crystalline SnS_2 nanoflakes were synthesized by facile low-temperature hydrothermal process. In a typical reaction process, aqueous solutions of 0.02 M $SnCl_4$ $5H_2O$ and 0.05 mol/L thiourea, both prepared in 50 mL DI water, were mixed well under constant stirring. After constant and vigerous stirring for 30 min, the resultant solution was transferred to teflon lined autoclave, sealed and heated upto 140 °C for 3 h. After desired reaction time, the autoclave was allowed to cool at room-temperature and finally yellowish precipitate was obtained which was extensively washed several times with DW, ethanol and acetone, sequentially and dried at 55 °C for 3 h. During the reaction, the thiourea reacts with water and produces H_2S which is further reacted with Sn^{4+} ions obtained from $SnCl_4$. The chemical reactions involved in the synthesis process can be written as:

$$NH_2CSNH_2+2H_2O \rightarrow 2NH_3+H_2S+CO_2$$

$$Sn^{4+}+H_2S \rightarrow SnS_2\downarrow+4H^+$$

The dried powder was then characterized in detail in terms of their morphological, structural and compositional properties and utilized as efficient photocatalyst for photocatalytic degradation of Rhodamine B and as an electron mediator for the fabrication of reproducible and highly sensitive nitro-aniline chemical sensor.

2.2. Characterizations of as-synthesized SnS_2 nanoflakes

The as-synthesized SnS_2 nanoflakes were characterized in detail by various analytical tools. The general and detailed morphologies of as-synthesized nanoflakes were done by field emission scanning electron microscopy (FESEM; JEOL-JSM-7600 F) and transmission electron microscopy (TEM) equipped with high-resolution TEM (HR-TEM). For HRTEM analysis, the synthesized products were ultrasonically dispersed in acetone and a drop of acetone solution, which contains the SnS_2 nanostructures, was placed on a copper grid and examined. The crystallinity and crystal phases were examined by the X-ray diffraction (XRD; PANanalytical Xpert Pro.) pattern measured with Cu-Kα radiation (λ = 1.54178 Å) in the range of 10–65°. The chemical composition of the as-synthesized SnS_2 nanoflakes was examined by Fourier transform infrared (FT-IR) spectroscopy, measured at room-temperature, in the range of 400–4000 cm^{-1}. To prepare the sample for FTIR measurements, small amount of the as-synthesized SnS_2 nanoflakes was mixed well with the potassium bromide (KBr) and subsequently compressed under high-pressure (~4 t) for pellet preparation. The obtained pellet, composed of SnS_2 nanoflakes and KBr, was used for the FTIR measurements.

2.3. Photocatalytic decomposition of rhodamine B dye using as-synthesized SnS_2 nanoflakes

The photocatalytic performance of the synthesized SnS_2 nanoflakes was examined by studying the photocatalytic decomposition of rhodamine B (RhB) dye. The photocatalytic degradation of RhB dye was performed under the illumination of Xenon arc lamp (300 W, Hamamatus: L 2479), attached with UV cut-off filter of wavelength 400 nm (FSQGG-400) which limited the illumination in a range of 400–800 nm, i.e. visible light. The degradation of RhB dye was calculated by measuring the UV–vis absorbance at 552 nm wavelength at certain time intervals. The photo-catalytic degradation was established in a 250 ml beaker using 150 ml of RhB dye solution (10 ppm). Prior to the light illumination, the prepared RhB dye solution was bubbled with oxygen for 30 min to allow the equilibrium of the system. For the photocatalytic experiments, 150 mg of the as-synthesized SnS_2 nanoflakes as photocatalyst were added to the RhB dye solution and stirred for 10 min for the initial physical adsorption of dye over SnS_2 nanoflakes surfaces. The decomposed dye solution was measured by using (UV–vis spectrophotometer Perkin Elmer-UV/VIS-Lambda 950) after regular time intervals.

2.4. Fabrication and characterization of nitro-aniline chemical sensor by I–V technique

To modify the electrode surface, firstly, the surface of glassy carbon electrode (GCE) was polished with commercially available alumina, followed by rinsing with DW thoroughly. For the GCE surface modification for nitro-aniline chemical sensor, slurry of SnS_2 nanoflakes were made by mixing an appropriate composition of SnS_2 nanoflakes and conducting agent (butyl carbital acetate). Finally, a small amount of the slurry was casted on GCE (surface area 0.0316 cm^2) surface, and then the modified electrode was dried in electric oven at 60 ± 5 °C for 4 h. The sensor analytical performance was investigated using *I–V* technique as discussed in our previous reports [25]. For *I–V* measurements, an electrometer (Keithley, 6517A, USA) was used as a voltage source and the SnS_2 nanoflakes/GCE was used as a working electrode while Pt wire was employed as a counter electrode. The current response was measured from 0.0 to 2.0 V while the time delaying and response time were 1.0 s and 10.0 s, respectively. The amount of 10.0 mL phosphate buffer solution was kept constant for all the measurements. For the concentration studies, a wide range of nitroaniline concentrations (15.6×10^{-6} mol/L–1×10^{-3} mol/L) was used. The sensitivity of the fabricated nitro-aniline chemical sensor was estimated from the slope of the current *versus* concentration from

the calibration plot divided by the value of active surface area of sensor/electrode. All the sensing experiments were carried out at room-temperature.

3. Results and discussion

3.1. Structural, morphological and compositional properties of SnS_2 nanoflakes

Prior to any applications, the as-synthesized SnS_2 nanoflakes were characterized in terms of their structural, morphological and compositional properties. To examine the crystallinity and crystal phase, the as-synthesized SnS_2 nanoflakes were examined by X-ray diffraction (XRD). Fig. 1 exhibits the typical XRD pattern for as-synthesized nanoflakes. All the reflections in the diffraction pattern are well matched with the typical SnS_2 crystals and can be indexed to the hexagonal SnS_2 phase with a lattice constant $a=3.649$ Å and $c=5.899$ Å. The observed XRD results are well matched with already reported literature (JCPDPS card no. 22–0951). Moreover, no other reflection, except SnS_2 reflections are seen in the pattern which confirms the formation of pure SnS_2 nanomaterials.

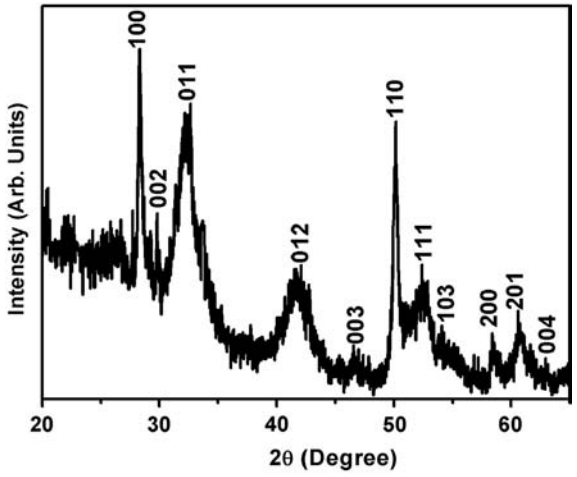

Fig. 1. XRD pattern of the as-synthesized SnS_2 nanoflakes prepared by facile hydrothermal process at low-temperature.

The general morphologies of as-prepared SnS_2 nanomaterials were examined by FESEM and shown in Fig. 2(a) and (b). Fig. 2 (a) exhibits the typical low-magnification image and revealed that the prepared SnS_2 nanomaterials possess flake-shaped morphology and are synthesized in large quantity. It is clear from the high-resolution images that the flakes are thin nanosheets which are curly in shape and randomly arranged (Fig. 2(b)). Moreover, due to larger size, the nanosheets are interconnected with each other in such a manner that they made some porous architecture structures and hence possess larger surface area. Therefore, these materials are promising candidates for photocatalysts and sensors applications. The typical thicknesses of the nanosheets are in the range of 60 ± 20 nm with several micrometers in width. The detailed morphological investigations of as-synthesized SnS_2 nanoflakes were examined by TEM equipped with high-resolution TEM (HRTEM). For the TEM analysis, the prepared SnS_2 nanoflakes were ultrasonically dispersed in acetone and a drop of acetone which contains the nanoflakes was placed on the TEM grid and examined.

Fig. 2(c) exhibits the typical low-resolution TEM image of the as-synthesized SnS_2 nanoflakes. It is clear from the TEM image that the nanoflakes were made by the thin SnS_2 nanosheets. Moreover, due to large size, the nanosheets are interconnected with each other which leads to the formation of some porous architecture. The typical thicknesses of the nanosheets are in the range of 60 ± 20 nm. It is also clear from the observed TEM image that the nanoflakes are synthesized in large quantity. All the TEM observations regarding shape, size and thickness are well matched with the obtained FESEM results. For further structural properties, the nanoflakes were investigated by HRTEM and results are shown in Fig. 2(d). The observed HRTEM exhibits a very clear and

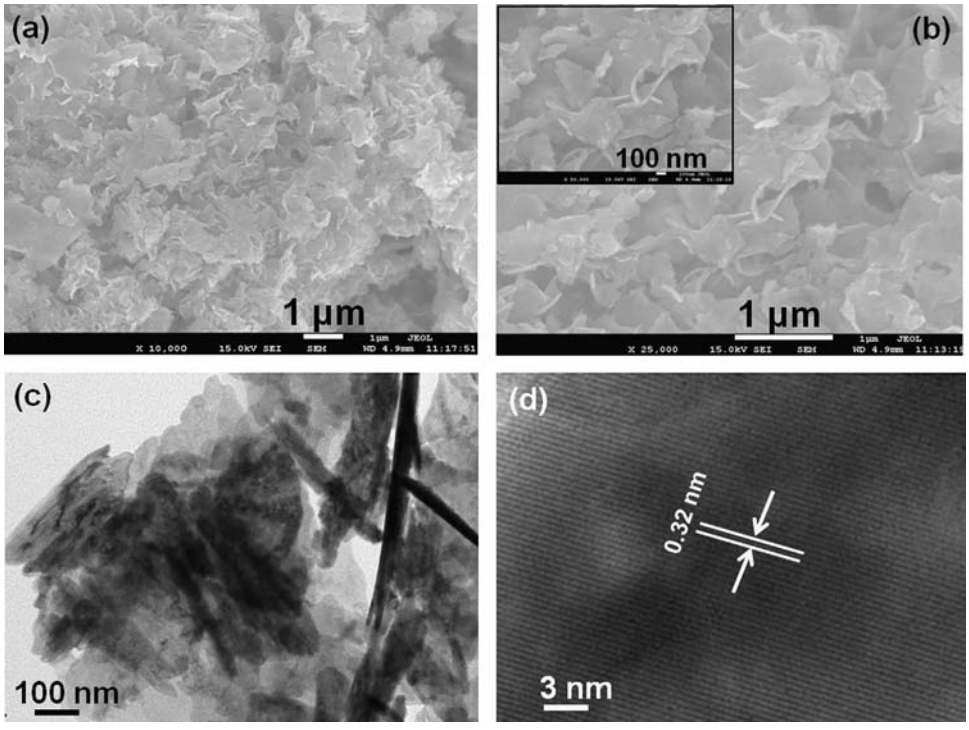

Fig. 2. (a) Low and (b) high-magnification FESEM, (c) low- and (d) high-resolution TEM images of the as-synthesized SnS_2 nanoflakes prepared by facile hydrothermal process at low-temperature.

well-defined lattice fringes with the lattice spacing of ~0.32 nm, which is fully consistent with the distance of (100) crystalline plane of the hexagonal SnS_2. The obtained HRTEM results are well matched with the XRD observations.

The chemical composition of as-synthesized SnS_2 nanoflakes was examined by using FTIR spectroscopy, as shown in Fig. 3. Several well-defined absorption bands were observed in the spectrum at 631, 1411 and 1641 cm^{-1}. The peak appeared at 631 cm^{-1} in the spectrum is due to the formation of Sn–S bond [26]. The origination of two very week peaks at 1411 and 1641 cm^{-1} are due to the formation of C–H and C–O bands, respectively [26]. Finally, due to the presence of Sn–S bond, it is confirmed that the synthesized nanomaterial is SnS_2.

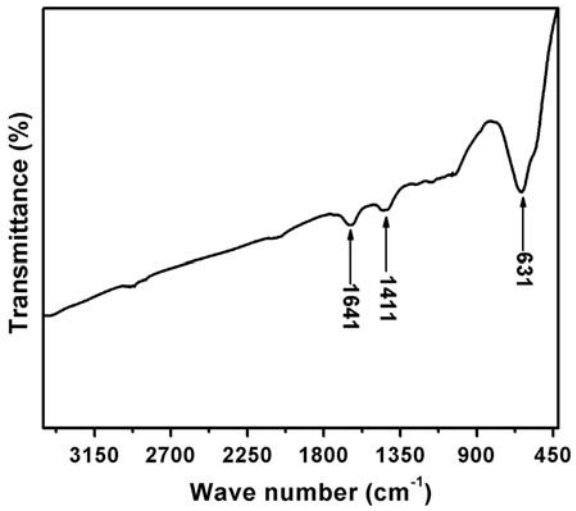

Fig. 3. FTIR spectrum of the as-synthesized SnS_2 nanoflakes prepared by facile hydrothermal process at low-temperature.

3.2. Visible-light driven photocatalytic properties of SnS_2 nanoflakes

To define the photocatalytic activity of synthesized SnS_2 nanoflakes, the degradation of RhB dye was performed under the visible light irradiation. The degradation rate of RhB dye was estimated by the following relation [27(a)];

$$\text{Degradation rate} = (A_0 - A/A_0) \times 100 = (C_0 - C/C_0)100$$

where, C_0 represents the initial concentration, C the variable concentration, A_0 the initial absorbance, and A the variable absorbance. Fig. 4 depicts the UV–vis absorption spectra (a), (b) % degradation rate versus time; (c) a plot for A_0/A versus time and (d) pie degradation chart of decomposed RhB dye solution by synthesized SnS_2 nanoflakes under the visible light irradiation. The photocatalytic degradation was monitored by measuring the maximum absorbance at the wavelength of 552 nm in regular time intervals (10 min) under visible light. Interestingly, it was observed that the relative absorption intensity continuously decreases as increasing the visible light exposure time which indicates that the RhB dye decomposes gradually over the surface of the photocatalyst, i.e. SnS_2 nanoflakes (Fig. 4(a)). Under visible light irradiation, the synthesized SnS_2 nanoflakes significantly degraded the RhB dye by ~61% within 120 min as shown in Fig. 4(b). However, the degradation rate of RhB dye was almost negligible when photocatalytic reaction is performed under visible light irradiation without SnS_2 nanoflakes which clearly suggested that the degradation rate increases in presence of the photocatalyst, i.e. SnS_2 nanoflakes. Fig. 4(c) shows the plot of the variation in the relative concentration (A/A_0) versus time interval for the photo-degradation of RhB dye over the surface of SnS_2 nanoflakes under visible light irradiation. Interestingly, the obtained results

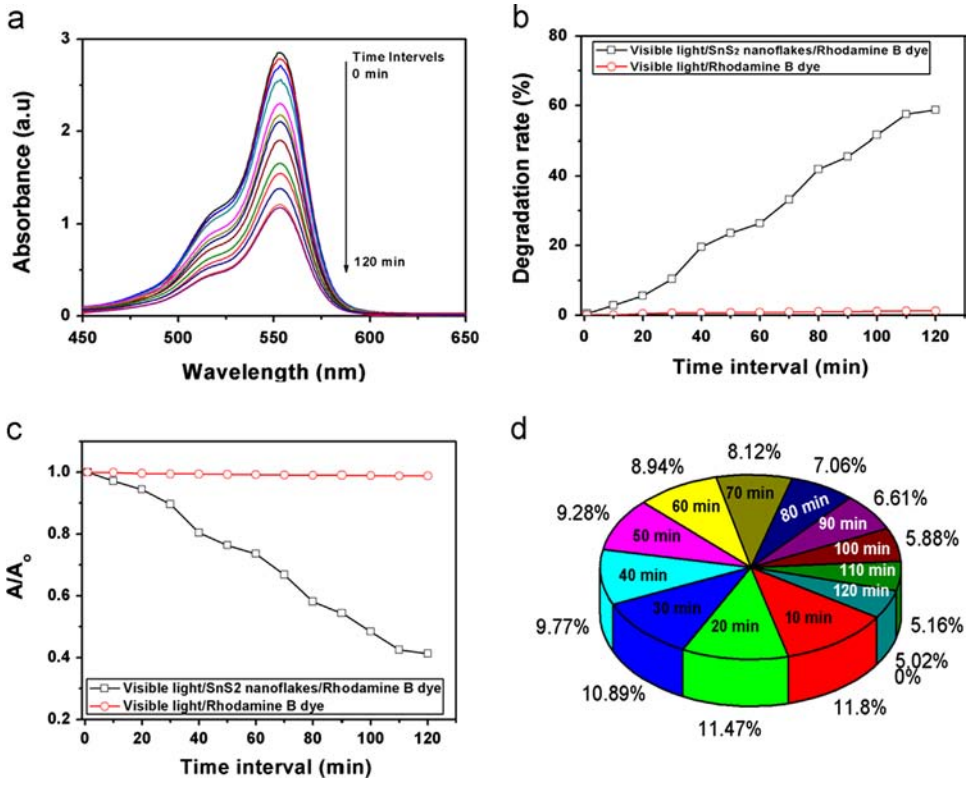

Fig. 4. (a) UV–Vis absorbance spectra of decomposed RhB dye solution over as-synthesized SnS_2 nanoflakes under visible light irradiation, (b) degradation rate (%) and (c) extent of decomposition (A/Ao) of RhB dye with respect to time intervals, (d) pie degradation chart of degraded RhB dye.

clearly display the gradual degradation of RhB dye over the surface of synthesized catalyst. The relative concentration of RhB dye decreases with increasing the visible light irradiation exposure time while in the absence of synthesized SnS_2 nanoflakes catalyst, negligible degradation is detected under visible light irradiation. The pie degradation chart of RhB dye (Fig. 4(d)) reveals that most of dye molecules are degraded in 80 min and afterward the degradation rate slows down. Conclusively, the synthesized SnS_2 nanoflakes as photocatalyst are able to degrade harmful RhB dye into the environment friendly residues under visible light irradiation. The mass spectroscopy of RhB dye before and after photocatalytic reaction has been examined to investigate the possible degradation products/intermediates of photocatalytic degradation of RhB dye, as shown in Fig. 5(a). At 0 min, RhB dye solution shows a strong mass signal at m/z=451.1, which is close to the mass of RhB dye. It is seen that a number of mass signals are detected in the RhB dye solution after 120 min, indicating the degradation of RhB dye over the surface of SnS_2 nanoflakes under visible light. The main mass signal at m/z=451.1 becomes weak after 120 min and splits into various mass signals. Fig. 5(b) depicts the possible degradation intermediates during the photocatalytic reactions which are illustrated on the observed mass signals. These possible reaction intermediates from fragmentations of the RhB dye contain the oxy groups in their rings. Thus, the formations of these intermediates might be helpful for the complete mineralization of organic dye [27(b)].

The schematic illustration to understand the degradation mechanism of RhB dye over the surface of SnS_2 nanoflakes was presented in Fig. 6. In general, the generation of oxyraicals such as hydroxyl ($OH^{\bullet}$) and superoxide ($O_2^{\bullet}$, $HO_2^{\bullet}$) are responsible for the degradation of organic dyes under light irradiation and these radicals are formed over the surface of semiconductors by the separation of electron–hole pairs [28]. Importantly, the presence of carbon species on surface of SnS_2 catalyst is responsible for creating active sites which is helpful for the degradation of dye under light illumination [29]. From the mechanism, upon light illumination SnS_2 nanoflakes absorbs the visible light and the electron ($\bar{e}$) from VB excites to CB which effectively causes a separation between $\bar{e}$

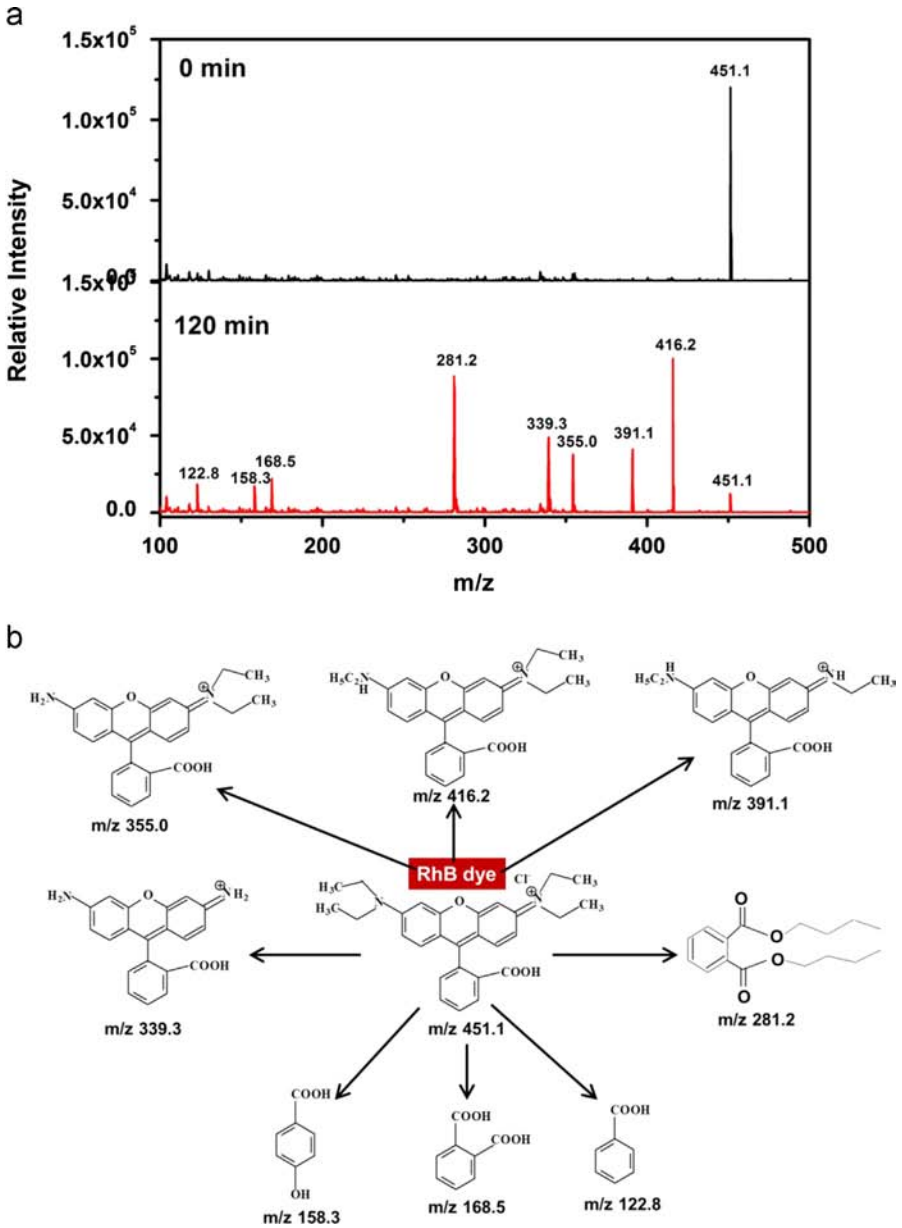

Fig. 5. (a) Mass spectra of RB dye solutions over as synthesized SnS_2 nanoflakes after 0 min and 120 min with the scan 100–500 m/z and (b) the possible reaction intermediates after the photocatalytic reaction.

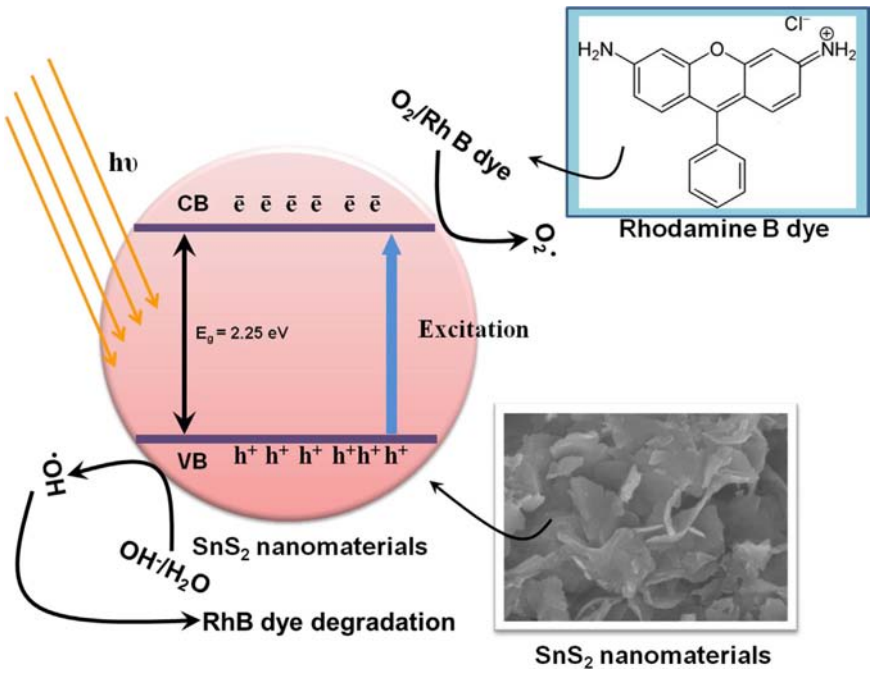

Fig. 6. A schematic illustration of photocatalytic activity of SnS_2 nanoflakes.

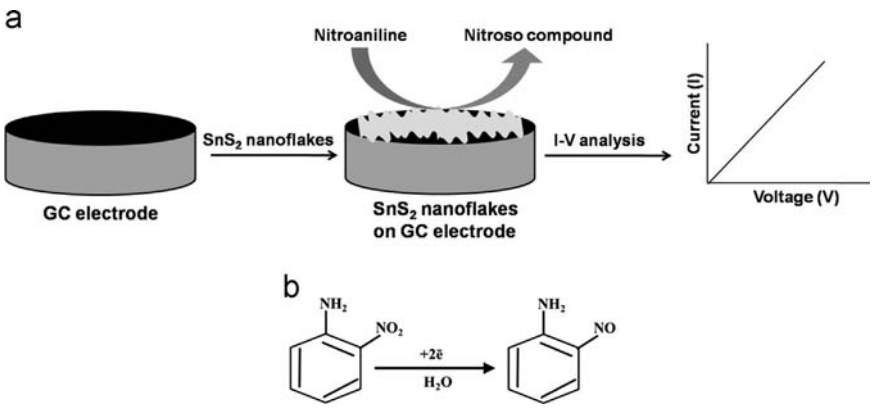

Fig. 7. (a) Schematic representation of nitroaniline chemical sensor fabricated based on *I–V* technique using SnS_2 nanoflakes modified GC electrode as working electrode; (b) chemical reaction describing the sensing mechanism.

and hole (h^+) pairs [30]. The RhB dye molecules firstly adsorb on the surface of the SnS_2 nanoflakes photocatalyst which reacts with water on the surface of SnS_2 nanoflakes photocatalyst to generate $RhB^{+\bullet}$ and $OH^{\bullet}$ radicals. The flakes morphology of synthesized SnS_2 nanomaterial sufficiently produces the large number of $RhB^{+\bullet}$ under visible light irradiation and credit to the easy transformation or oxidation of harmful organic dye into less harmful chemicals. Moreover, the unique band gap and large surface area (34.6 m^2/g) of synthesized SnS_2 nanoflakes photocatalyst could able to provide efficient $\bar{e}$ and h^+ separation, resulting in the formation of large number of $RhB^{+\bullet}$ and $OH^{\bullet}$ radicals [31]. In this work, the high degradation of RhB dye is due to morphologies of nanoflakes and generation of $RhB^{+\bullet}$ and $OH^{\bullet}$ radicals on the surface of SnS_2 nanoflakes.

3.3. Nitroaniline chemical sensor application of as-synthesized SnS_2 nanoflakes

The detailed methodology to modify the GC electrode with SnS_2 nanoflakes is described in experimental details section. Fig. 7 (a) exhibits the schematic representation of nitro-aniline chemical sensor fabricated based on SnS_2 nanoflakes coated GCE electrode and its sensing mechanism by I-V technique. Briefly, slurry of SnS_2 nanoflakes was made by mixing it with appropriate amount of binder and casted on GC electrode. In two electrode system, the SnS_2 modified electrode was used as working electrode while the Pt wire was employed as counter electrode. The current (*I*)–voltage (*V*) measurements have been carried out to evaluate the sensing properties such as sensitivity, detection limit, correlation coefficient, etc of SnS_2 nanoflakes electrode towards nitroaniline chemical. Fig. 7 (b) shows the proposed mechanism of nitroaniline sensing over the SnS_2 nanoflakes electrode. The detection of nitroaniline chemical over the surface of SnS_2 nanoflakes electrode might explain by the push-pull system which depends on the existing functional groups in conjugated π–π backbone [32]. In case of nitroaniline, the amino group acts as electron donor or pushing group and nitro group acts as electron acceptor or pulling group. In electrochemical system or sensor, the active sites on the surface of SnS_2 nanoflakes electrode are easily attracted amino group [33]. On the other hand, nitro group recombines with $\bar{e}$ and simultaneously reacts with H_2O to form non harmful nitroso compound which responses in the *I–V* measurements in the form of increment of current.

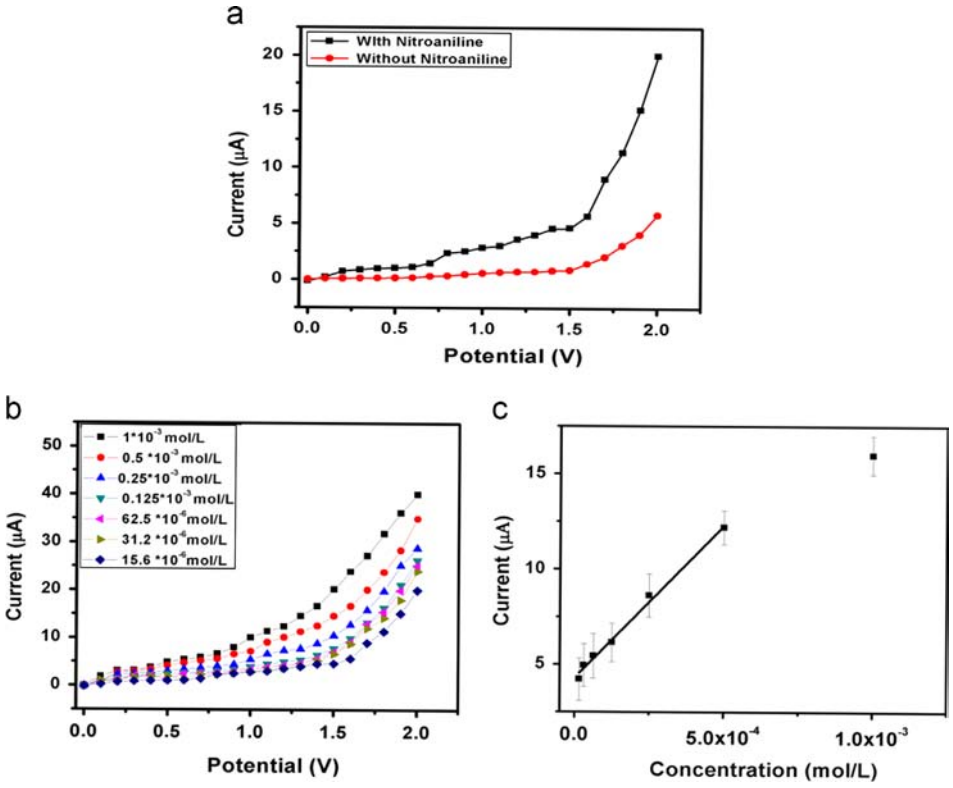

Fig. 8. (a) Typical *I–V* responses of SnS_2 nanoflakes in (GCE) in 10 ml, 0.1 mol/L PBS solution, (■) with nitro-aniline (15.6×10^{-6} mol/L) and (●) without nitro-aniline; (b) *I–V* response for various concentrations of nitro-aniline (from 15.6×10^{-6} mol/L to 1×10^{-3} mol/L) and (c) calibration curve.

Fig. 8(a) depicts the I–V measurements of the fabricated chemical sensor based on SnS_2 nanoflakes modified GC electrode without and with nitro-aniline. A sharp increase in the current of ~20.3 μA is observed after the addition of nitro-aniline (15.6×10^{-6} mol/L) as compared to chemical sensor without nitro-aniline, suggesting the electrocatalytic activity of SnS_2 electrode towards the nitro-aniline chemical. The sensing parameters of fabricated nitro aniline chemical sensor with SnS_2 nanoflakes electrode are evaluated by performing a series of the *I–V* measurements with different concentration of nitro-aniline in PBS. To the best of our knowledge, it is the first report on the sensing behavior of SnS_2 nanoflakes electrode towards the detection of nitro-aniline. To investigate the detailed sensing performance of the SnS_2 nanoflakes modified electrode, systematic *I–V* measurement experiments have been done by varying the concentration of nitro-aniline in 10 ml of PBS (0.1 M). Fig. 8(b) exhibits the *I–V* responses of SnS_2 nanoflakes modified GCE towards various concentrations of nitro-aniline (from 15.6×10^{-6} mol/L to 1×10^{-3} mol/L). It is clear from the observed graph that the current gradually increases as increasing the nitro-aniline concentrations ranging from ~15.6×10^{-6} mol/L to 1×10^{-3} mol/L which reveals that the modified SnS_2 nanoflakes electrode based chemical sensor presents the good sensing response to the nitro-aniline. It is reported that incremental enhancement in current is related to the generation of ions and enlargement in ionic strength of PBS solution. In our case, the incremental addition of nitro-aniline might generate the large number of ions and hence increase the ionic strength of the solution. To evaluate the sensitivity of the fabricated sensor, a calibration curve of current versus nitro-aniline concentrations has been plotted and shown in Fig. 8(c). Importantly, the calibrated current linearly increases up to the nitro-aniline concentrations of ~0.5×10^{-3} mol/L. This phenomenon suggests the good linearity of fabricated chemical sensor based on SnS_2 nanoflakes electrode in the range of 15.6×10^{-6} mol/L–0.5×10^{-3} mol/L. In other words, the unique nanoflakes morphology of SnS_2 might provide the enough active sites over the surface of modified electrode, which results the high adsorption of nitro-aniline through SnS_2 nanoflakes electrode. The sensitivity of fabricated nitro-aniline sensor was estimated by the slope of the calibrated current curve. A high and a reproducible sensitivity of ~505.82 ± 0.02 mA cm^{-2}.(mole/L)$^{-1}$ with the experimental detection limit of ~15×10^{-6} mol/L in a short response time of ~10.0 s is achieved by the fabricated nitro-aniline chemical sensor based on SnS_2 nanoflakes electrode.

To examine the reproducibility and stability of the fabricated chemical sensor based on SnS_2 nanoflakes electrode, the sensing responses of the fabricated sensor was measured for three consecutive weeks. After each experiment, the fabricated sensor was stored in phosphate buffer solution (pH=7.0). Interestingly, no significant decrease was observed in the sensing parameters for three weeks which conclude that the fabricated sensor possess good reproducibility and stability. Finally, due to very specific morphology and various interesting physical and chemical properties, it is proposed that of SnS_2 nanoflakes is very potential, promising and effective electrocatalytic material for the detection of hazardous chemicals like nitro-aniline.

4. Conclusion

In summary, well-crystalline SnS_2 nanoflakes have synthesized by facile hydrothermal process at low-temperature. The detailed studies reveal that the synthesized products are well-crystalline nanoflakes and are grown in large quantity. The synthesized SnS_2 nanoflakes are used as efficient photocatalyst for photocatalytic degradation of Rhodamine B dye and as an electron mediator for the fabrication of reproducible and highly sensitive nitro-aniline chemical sensor. The photocatalytic degradation based on SnS_2 nanoflakes photocatalyst of Rhodamine B dye under visible light irradiation exhibit about 61% degradation. The fabricated chemical sensor exhibits a very high sensitivity of ~505.82 ± 0.02 mA.cm^{-2}.

(mole/L)$^{-1}$ and experimental detection limit of $\sim 15 \times 10^{-6}$ mole/L in a short response time of ~10.0 s. This research exhibits that the synthesized SnS_2 nanoflakes can effectively be used as visible-light-driven photocatalysts and chemical sensors applications.

Acknowledgements

Authors would like to acknowledge the support of the Ministry of Higher Education, Kingdom of Saudi Arabia for this research through a grant (PCSED-001–11) under the Promising Centre for Sensors and Electronic Devices (PCSED) at Najran University, Kingdom of Saudi Arabia. M.S. Akhtar acknowledge the Research Funds of Chonbuk National University in 2011.

References

[1] H.S. Nalwa, Encyclopedia of Nanoscience and Nanotechnology, 11–25 ed., American Scientific Publishers, USA, 2011.
[2] T.Y. Tseng, H.S. Nalwa, Handbook of Nanoceramics and Their Based Nanodevices, 1–5, American Scientific Publishers, USA, 2009.
[3] B. Jia, W. Jia, X. Wu, F. Qu, Sci. Adv. Mater. 4 (2012) 1127–1133.
[4] (a) Y. He, Chin. Particuol. 2 (2004) 168;
(b) B. Jia, W. Jia, Y. Ma, X. Wu, F. Qu, Sci. Adv. Mater. 4 (2012) 702–707.
[5] (a) E. Hu, Y.Z. Wang, Chemosphere 39 (1999) 2107;
(b) S.S. Arbuj, R.R. Hawaldar, S. Varma, S.B. Waghmode, B.N. Wani, Sci. Adv. Mater. 4 (2012) 568–572.
[6] (a) G.M. Colonna, T. Caronna, B. Marcandalli, Dyes Pigm. 41 (1999) 211–220;
(b) D. Tassalit, A.N. Laoufi, F. Bentahar, Sci. Adv. Mater. 3 (2011) 944–948.
[7] (a) K.P. Mishra, P.R. Gogate, J. Environ. Manage. 92 (2011) 1972–1977;
(b) Q. Sun, Y. Lu, Y. Liu, J. Nanoeng. Nanomanuf. 2 (2012) 46–48.
[8] (a) O.J. Hao, H. Kim, P.C. Chiang, Environ. Sci. Technol. 30 (2000) 449–505;
(b) L.S. Roselin, R. Selvin, Sci. Adv. Mater. 3 (2011) 113–119;
(c) Z. Jin, G.T. Fei, X.Y. Hu, M. Wang, L.D. Zhang, J. Nanoeng. Nanomanuf. 2 (2012) 49–53.
[9] (a) P.R. Gogate, A.B. Pandit, AIChE J. 50 (2004) 1051–1079;
(b) H.G. Oliveira, B.C. Fitzmorris, C. Longo, J.Z. Zhang, Sci. Adv. Mater. 4 (2012) 673–680;
(c) S. Barreca, S. Orecchio, A. Pace, Talanta 103 (2013) 349–354.
[10] (a) H.X. Li, X.Y. Zhang, Y.N. Huo, J. Zhu, Environ. Sci. Technol. 41 (2007) 4410;
(b) P. Tang, H. Chen, F. Cao, G. Pan, K. Wang, M. Xu, Y. Tong, Mater. Lett. 65 (2011) 450–452;
(c) Y.C. Zhang, Z.N. Du, K.W. Li, M. Zhang, Sep. Purif. Technol. 81 (2011) 101–107.
[11] (a) J.C. Colmenares, M.A. Aramendia, A. Marinas, J.M. Marinas, F.J. Urbano, Appl. Catal. A 306 (2006) 120;
(b) Thaís M. Milao, Vagner R. de Mendonça, Vinícius D. Araújo, W. Avansi, C. Ribeiro, E. Longo, M.I. Bernardi, Sci. Adv. Mater. 4 (2012) 54–60.
[12] H. Zhang, R.L. Zong, J.A. Zhao, Y.F. Zhu, Environ. Sci. Technol. 42 (2008) 3803.
[13] W.M. Du, J. Zhu, S.X. Li, X.F. Qian, Cryst. Growth Des. 8 (2008) 2130.
[14] N.Z. Bao, L.M. Shen, T. Takata, K. Domen, Chem. Mater. 20 (2008) 110.
[15] A. Agarwal, P.D. Patel, D. Lakshminarayana, J. Cryst. Growth 142 (1994) 344.
[16] V.V. Ivanovskaya, A.N. Enyashin, A.L. Ivanovskii, J. Struct. Chem. 45 (2004) 151.
[17] T. Brousse, S.M. Lee, L. Pasquereau, D. Defives, D.M. Schleich, Solid State Ionics 151 (1998) 51.
[18] D.B. Mitzi, J. Mater. Chem. 14 (2004) 2355.
[19] G. Domingo, R.S. Itoga, C.R. Kannewurf, Phys. Rev. 143 (1966) 536.
[20] C.D. Lokhande, J. Phys. D 23 (1990) 1703.
[21] (a) T. Jiang, G.A. Ozin, J. Mater. Chem. 8 (1998) 1099;
(b) J. Chao, Z. Xie, X.B. Duan, Y. Dong, Z. Wang, J. Xu, B. Liang, B. Shan, J. Ye, D. Chen, G. Shen, Cryst. Eng. Commun. 14 (2012) 3163–3168.
[22] (a) X.L. Gou, J. Chen, P.W. Shen, Mater. Chem. Phys. 93 (2005) 557;
(b) Xi Li, J. Zhu, H. Li, Appl. Catal. B Environ. 123–124 (2012) 174–181.
[23] (a) C. Yang, W. Wang, Z. Shan, F. Huang, J. Solid State Chem. 182 (2009) 807–812;
(b) Y.C. Zhang, Z.N. Du, K.W. Li, M. Zhang, Sep. Purif. Technol. 81 (2011) 101–107.
[24] (a) D. Vollath, D.V. SzabO, Acta Mater. 48 (2000) 953;
(b) Y.C. Zhang, J. Li, M. Zhang, D.D. Dionysiou, Environ. Sci. Technol. 45 (2011) 9324–9331.
[25] A. Umar, F. Al-Hazmi, G.N. Dar, S.A. Zaidi, R.M. Al-Tuwirqi, F. Alnowaiserb, A. A. Al-Ghamdi, S.W. Hwang, Sens. Actuat. B Chem. 166–167 (2012) 97–102.
[26] (a) K. Nakamoto, IR Spectra of Inorganic and Coordination, Compounds-2nd Ed., Wiley Eastern NY, 1970;
(b) R.A. Nyquist, R.O. Kagel, Infrared Spectra of Inorganic Compounds, Academic Press, Inc., New York, London220.
[27] (a) L.X. Zhang, P. Liu, Z.X. Su, Polym. Degrad. Stab. 91 (2006) 2213;
(b) L. Xueyan, W. Desong, C. Guoxiang, L. Qingzhi, A. Jing, W. Yanhong, Appl. Catal. B Environ. 81 (2008) 267–273.
[28] (a) S. Ameen, M.S. Akhtar, Y.S. Kim, H.S. Shin, Appl. Catal. B Envron. 103 (2011) 136–142;
(b) X.Y. Li, D.S. Wang, G.X. Cheng, Q.Z. Luo, J. An, Y.H. Wang, Appl. Catal. B 81 (2008) 267.
[29] (a) T.A. Saleh, V.K. Gupta, J. Coll. Interf. Sci. 371 (2012) 101–106;
(b) L. Fuks, D. Filipiuk, M. Majdan, J. Mol. Struct. 792–793 (2006) 104–109.
[30] Y. Li, J. Hagen, D. Haarer, Synth. Mat. 94 (1998) 273.
[31] S.A. Khayyat, M.S. Akhtar, A. Umar, Mater. Lett. 81 (2012) 239–241.
[32] M.M. Miranda, N. Neto, Colloids Surf. A 249 (2004) 79.
[33] B.C. Roy, M.D. Gupta, J.K. Ray, Macromolecules 28 (1995) 1727.